ACS ES&T Air

pubs.acs.org/estair Article

Evaluating Field Performance Thresholds for Aerial Methane Technologies Using Large-Scale Field Measurements

Saahil Gupta, Erin Tullos, David Lyon, Haoming Ma, and Arvind P. Ravikumar*

Cite This: https://doi.org/10.1021/acsestair.5c00437 Read Online

ACCESS | Metrics & More | Article Recommendations | Supporting Information

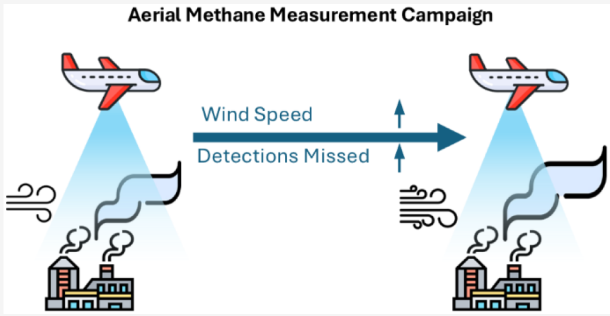

ABSTRACT: Mitigating methane from the oil and gas supply chain is a feasible and effective way to address global warming over the next decade. Aerial measurement campaigns have been extensively deployed to detect and quantify methane emissions from oil and gas facilities to inform and assess the effectiveness of mitigation activities. While performance benchmarks of these technologies have been evaluated under controlled conditions, they have not been widely validated under field conditions. Understanding the impact of ambient conditions, such as wind, on the performance of aerial detection technologies is essential not only for assessing their ability to detect emission sources, but also for interpreting the measurements. Accurate quantification of emissions requires estimating the portion of emissions that may be missed. In this work, we present a method to determine a field performance threshold, which reflects the magnitudes of emissions that these technologies can detect under real-world operating conditions. Our results show that wind speeds have a more pronounced impact on minimum detection limits than predicted by analytical models or probability of detection curves built from controlled test results. We find that under varied field conditions, approximately 18% of emissions may not be observed, compared to what would be expected from minimum detection limits established through controlled release experiments. A field performance threshold offers a more representative metric for evaluating performance and guiding the interpretation of results from field measurement campaigns.

KEYWORDS: *methane emissions, oil and gas, aerial measurement, probability of detection, meteorological parameters*

1. INTRODUCTION

Methane (CH_4) emissions from human activity represent a critical challenge in global climate mitigation efforts.[1] Methane has a short lifetime but is a potent greenhouse gas (GHG), whose emissions have led to a 0.5 °C warming over 2010–2019 relative to 1850–1900 levels.[2] Methane emissions from the oil and gas sector are a significant component of the global methane budget with recent studies finding that these emissions are underreported by up to 60% globally.[3] The United States is the largest global emitter of methane from oil and gas operations but studies suggest that 50% of these methane emissions can be mitigated at no net cost using existing technologies.[4] Near-term action to lower methane emissions will also lead to better air quality outcomes by reducing coemitted pollutants.[2] The European Commission and 159 countries have signed on to the Global Methane Pledge (GMP) to reduce global methane emissions by at least 30% from 2020 levels by 2030.[5] In addition, several voluntary initiatives such as the Oil and Gas Methane Partnership (OGMP) have been launched that encourage measurement, reporting, and verification (MRV) of methane emissions.[6]

Aerial methane detection technologies have become a central tool for characterizing emissions across U.S. oil and gas basins at multiple spatial scales. These field campaigns have demonstrated the importance of large emitters in contributing to a majority of methane emissions at the source-, site-, and regional scales.[7−18] The Permian Basin has been the focus of numerous studies aimed at estimating methane leakage rates, with reported results exhibiting both substantial variability and some of the highest values among U.S. oil and gas basins.[8,10,11,13,19,20] Cusworth et al. (2021) highlight the substantial variability in measured emissions across repeated campaigns. During seven separate Airborne Visible-Infrared Imaging Spectrometer-Next Generation (AVIRIS-NG) overflights in the Delaware sub-basin, annual CH_4 emission estimates varied from 0.54 to 1.04 Tg/a.[10] Four Carbon Mapper measurement campaigns over the Permian Basin from 2019 to 2021 estimated natural gas loss rate estimates varying from 2% to 5%.[20] Chen et al. (2020) analyzed data collected at

Received: November 3, 2025
Revised: May 25, 2026
Accepted: May 27, 2026

91.2% of active wells in the New Mexico portion of Permian using Kairos' infrared imaging spectrometer.[19] They concluded that 50% of emissions originated from large sources emitting more than 380 t/h, showing a gas production normalized leakage rate of 9.4%.[19]

Measurements collected by different aerial methane measurement technologies when deployed over similar spatial and temporal scales often capture varying subsets of the full emissions distribution.[8,21] For example, Kunkel et al. (2023) analyzed imaging spectrometer data from both Bridger Photonics' Gas Mapping LiDAR (GML) and Carbon Mapper instruments - Global Airborne Observatory (GAO), AVIRIS-NG collected across the Permian Basin between 2020 and 2021. The combined data sets revealed that Carbon Mapper identified 1.48% of surveyed sites as emitters, whereas Bridger identified 38.3%. The field based detection limit for Carbon Mapper in the Permian Basin at 50% detection ratio is 280 kg/h and 90% of the emissions are above 249 kg/h whereas for Bridger GML 90% of the emissions are above 16.9 kg/h.[8] Similarly, Stokes et al. (2022) compared Bridger GML with Scientific Aviation's aerial mass balance quantification approach over Permian Basin facilities in West Texas. Bridger reported a higher proportion of low-emitting sites (<10 kg/h; 29%) compared to Scientific Aviation (6%), while Scientific Aviation reported a higher proportion of high-emitting sites (>10 kg/h; 27%) versus Bridger (14%).[21] These differences suggest that each technology detects a specific subpopulation of the total emissions occurring during the observation period. When comparing emissions across large numbers of sites, differences in observed distributions are generally attributable to differences in both detection thresholds and measurement techniques. In contrast, differences in measurements taken at the same site but not at precisely the same time may also reflect temporal variability in emissions, rather than differences in technology alone. Ultimately, observed differences are likely driven by a combination of factors, including variation in minimum detection limits, differing approaches to emissions quantification (e.g., plume imaging versus point sensing), and the dynamic nature of emission sources.

An analysis of the top nine oil and gas producing basins in the US concluded that the majority of methane emissions, ranging from 63% to 90%, come from facilities emitting less than 100 kg/h.[22] The uncertainty in contribution from small and large emitters in oil and gas basins underlines the need to include low-emission rate sources in comprehensive methane emission assessments. Measurement strategies must therefore include the capability to accurately capture both high-magnitude emissions from superemitters and low-magnitude emissions from smaller sources. Additionally, the variability in detection rates between technologies highlights the importance of identifying and addressing differences in their measurement capabilities.

Several studies have evaluated the performance characteristics of aerial methane measurement technologies.[23−29] Recent controlled release testing has shown that most aerial platforms can reliably detect emissions down to 10 kg/h, with some even detecting emissions below 3 kg/h under ideal conditions.[29] While controlled release testing is essential for quantifying baseline detection capabilities, it does not fully capture how these technologies perform under variable real-world operating conditions. A study to assess the probability of detection (PoD) threshold of a methane measurement satellite shows that the detection limit in the field is 250−350 kg/h as opposed to a stated minimum detection limit of 100 kg/h. The study also notes that single blind releases may not be temporally distributed sufficiently to capture potential seasonal influences on plume retrieval conditions.[30] In principle, detection limits and PoD curves derived from controlled tests should allow researchers to account for emissions that fall below the field performance threshold. However, analysis of large field data sets reveals that the apparent emissions distributions from smaller sources vary with ambient conditions, particularly wind speed. Across previous studies, smaller sources are present but are not uniformly detected, indicating that field detection performance is likely influenced by local environmental conditions resulting in variable probability of detection curves. These findings point to a persistent challenge in reconciling controlled test results with operational field performance. Moreover, there remains a lack of validation of field measurements against PoD curves derived from controlled releases, leaving uncertainty around what proportion of total emissions is being missed in measurement campaigns.

In this work, we address this gap by quantifying the differences in performance of two commonly used aerial methane technologies - Carbon Mapper and Bridger Photonics GML - between controlled test settings and field deployment in the Permian Basin. While earlier studies have primarily focused on controlled release experiments to evaluate minimum detection limits, quantification accuracy, and retrieval algorithm performance, others have concentrated on characterizing emissions distributions at scales ranging from individual facilities to entire basins.[7−18,23−29] These two types of studies have remained largely distinct, limiting the ability to understand whether performance parameters derived through controlled releases translate to broader field campaigns. Kunkel et al. (2023) suggests that field detection performance can differ from the minimum detection limit developed from controlled release tests. However, it focuses on constructing a basin-scale emissions distribution for the Permian Basin, rather than evaluating the factors that influence emissions detection near the detection threshold.[8] Our findings show that there is a consistent upward linear trend in the field performance threshold with increasing local wind speed, and emissions are likely to be underestimated at very low and high wind speeds. Validation of field results with controlled release studies and probability of detection (PoD) equations highlights areas of discrepancies. Our results indicate that the underperformance during field campaigns relative to controlled-release benchmarks is most pronounced near the minimum detection limit of each technology. We show that large field-campaign data sets can be used to characterize field detection behavior including near-threshold detection performance. This complements and extends insights from controlled-release testing without requiring exhaustive new controlled-release experiments for every basin and season. These findings are critical for refining technology deployment strategies and improving detection reliability in real-world conditions.

2. METHODS

We assess two airborne methane detection technologies - Carbon Mapper (AVIRIS-NG and GAO) and Bridger Gas Mapping LiDAR (GML). Carbon Mapper is an aircraft-based platform that detects and quantifies methane emissions across large areas. The platform uses passive infrared spectrometry to detect and quantify methane emissions by analyzing the attenuation of surface reflected light,

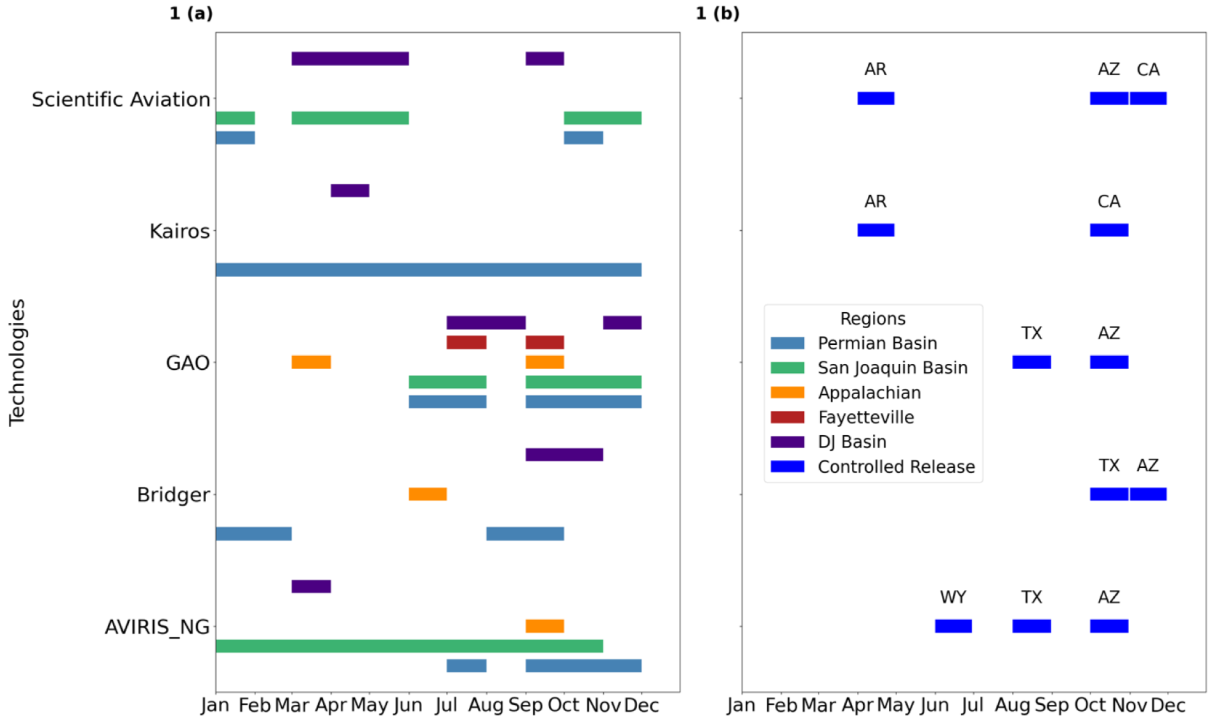

Figure 1. (a) Timeline of the deployment of aerial methane measurement technologies across basins in the US—Permian (blue),[8,10,11,13,14,19,21,22] San Joaquin (green),[9,38] Appalachian (orange),[22,39] Fayetteville (red),[40] Denver-Julesburg (purple);[41] (b) Timeline for controlled release tests (blue) across the US for the five technologies.[23,26−29,32−34,40,42,43] The analyses in this paper focus on Carbon Mapper and Bridger GML in the Permian Basin due to availability of comparable field data sets.

where returned light intensity at certain wavelengths is diminished due to absorption by methane. The platform's detection capabilities allow it to identify emissions down to 10 kg/h when tested in a controlled release experimental setup.[29]

Field performance threshold is an empirical, basin-specific effective threshold inferred from the field data sets for a particular technology. It represents the lower end of emission rates that are reliably observed under the local environmental conditions (equated in this paper to the median of the lowest 10th percentile of emissions) detected in that basin and season. Detection performance may be influenced by local conditions, and we do not assume that this field threshold is standard across basins. This field threshold is distinguished from the minimum detection limit which is the detection limit as a function of wind speed that is developed from controlled release tests. Controlled methane releases are used to estimate detection performance across various conditions and the results are regressed into a probability of detection (PoD) equation as a function of wind speed (and other factors where applicable). The minimum detection limit we use corresponds to the 90% probability of detection (PoD) threshold at a particular wind speed, following prior studies in this field.[31]

A field study to assess oil and gas emissions in the Permian Basin shows that the field performance threshold varies between 70 and 150 kg/h during a 3-week campaign in the summer.[31] Thorpe et al. (2016) conducted controlled release experiments to assess AVIRIS-NG's effectiveness in detecting methane point sources with flight altitudes spanning between 430 and 3800 m Above Ground Level (AGL) and wind speeds ranging from 0.66 to 7.5 m/s.[33] We expect the detected emissions during field campaigns to largely follow the models developed using statistical regression to define a predictor function that accounts for methane release rate, wind speed, and flight altitude.[33] We use a rearranged form of this equation solved for emission rate as a function of the other variables.

$$Q = \left(\left(\frac{1}{1 - PoD_{CM}}\right)^{1/3} - 1\right) \times \frac{1}{31.1 \times 10^{-3}} \times \left(\frac{h}{1000}\right)^{1.91} \times \exp(0.239u)^{1/1.99} \quad (1)$$

Here, Q represents the emission rate in kg/h, PoD_{CM} represents the Probability of Detection for AVIRIS-NG, h is the flight altitude in m, and u is the local wind speed in m/s.

Bridger Photonics' Gas Mapping LiDAR (GML) is an airborne methane detection technology that uses a topographic LiDAR system. Methane is detected and quantified by measuring the attenuation of reflected light at specific wavelengths using frequency-modulated lasers that operate within a methane absorption band. Under optimal conditions, the technology performs with a minimum detection limit of 1 kg/h.[26,34] A deployment invariant PoD model for Bridger GML has been developed by Thorpe et al. (2024).[27] The model incorporates emission rate, wind speed, and gas concentration noise (GCN) as key predictors and generalizes the results across deployment configurations and environmental conditions. The dependence of emissions detection on the altitude of the flight is incorporated in the two GCN parameter values developed by Thorpe et al. (2024). In our analyses, we use both GCN values, so any altitude dependence is included in our results. The inverse PoD model for Bridger GML developed from controlled release studies at Midland, Texas is shown in an adapted form in eq 2.[27]

$$Q = \left(\frac{GCN^{2.7501} \times u^{2.0877}}{2.998 \times 10^{-4}} \exp(\sqrt{2} \times 0.8326 \times \operatorname{erfinv}(2 \times PoD_{B\_GML} - 1) + (-0.3466))\right)^{1/2.6339} \quad (2)$$

Here, Q represents the emission rate in kg/h, u is the local wind speed in m/s, GCN is the gas concentration noise (13 ppm-m and 22 ppm-m), and PoD_{B_GML} represents the Probability of Detection for Bridger Gas Mapping LiDAR.

https://doi.org/10.1021/acsestair.5c00437
ACS EST Air XXXX, XXX, XXX−XXX

Both technologies use different light sources, and their minimum detection limits depend on the source strength and the chosen wavelength region. Bridger GML uses an active light source and Carbon Mapper relies on passive light refelcted from the sun. This allows for a comparative analysis of the effect of the various meteorological factors on detection by the two technologies. The rationale for choosing these technologies is their widespread deployment at oil and gas sites and their effectiveness in detecting methane emissions across a range of scales, from facility-level leak detection to basin-wide emissions estimates. Both technologies have been extensively deployed in measurement campaigns over the Permian Basin. Details of deployment over different basins across the United States is discussed in Section 3.1.

For Carbon Mapper, measurement data is publicly available for the Permian Basin field campaigns conducted in the summer of 2020 and the fall of 2021. Local meteorological factors such as wind speed, solar irradiance, and albedo were gathered at the locations of plume detection for Carbon Mapper measurements. Meteorological data is obtained from the National Oceanic and Atmospheric Administration (NOAA) via the Meteostat API.[35]

For the Bridger GML analysis, we use data collected during four phases of field campaigns conducted in the Permian Basin in 2021 and 2022.[36,37] The Bridger GML and Carbon Mapper data sets used in this analysis are based on individual overflights (single-scan detections), not site-averaged values. Each detection corresponds to a single pass over a facility, so the data sets for the two measurement technologies are directly comparable in this regard. Bridger GML is analyzed using meteorological data derived from the nearest airport Meteorological Aerodrome Report (METAR) surface observation (measured by an Automated Surface Observing System (ASOS)) since plume detection coordinates were not available. The Midland Airport in Texas and Carlsbad Airport in New Mexico serve as representative locations for the meteorological factors. The Supporting Information (SI) Section S4 includes a comparative analysis to evaluate the validity of using representative airport data by comparing Carbon Mapper's results derived directly from plume locations with those based on airport data. Since the wind speeds taken from nearby airports may be noisy and may not represent the wind speed transporting the plumes, this comparison assesses whether the airport-based meteorological data can reliably substitute for local wind speed values in accurately quantifying emissions. Based on the comparison with location-specific winds, the average relative uncertainty is ~80% near Midland TX and ~200% near Carlsbad NM. The implications of wind speed error on emissions detection are discussed in Section S5. Generally, Bridger GML incorporates meteorological data at a finer spatial and temporal resolution than available from the nearest airport.

We analyzed the detection performance of both aerial technologies with respect to local wind speed, albedo, temperature, and solar zenith angle. Wind speed emerged as the dominant factor affecting the field performance threshold. The other parameters exerted less influence, and their effects on detection performance are described in the SI Sections S2 and S3. The comparison between emissions data from field campaigns and controlled settings is quantified using regression analyses and confidence intervals. The resulting coefficients are used to determine the extent of the discrepancy between expected minimum detection limits from PoD curves and the field performance threshold to assess real world performance. To highlight the emissions that are more likely to be missed in field settings, emissions data is grouped into bins based on the local wind speed magnitude and the 10th percentile emissions are also identified. A comparative analysis of the distributions of the true and detected emissions allows for the quantification of specific range of emissions that may be under-represented or missed in field campaigns.

3. RESULTS

3.1. Comparing Deployment Timelines across Basins

Figure 1 shows a deployment timeline to track the specific times and locations where five different aerial methane measurement technologies are deployed across major US oil and gas basins. The timeline indicates the potential seasonal effects on emissions detection by showing when each technology was deployed in the field. In Figure 1a, there are specific time blocks when technologies such as Bridger GML and Carbon Mapper (AVIRIS-NG and GAO) are deployed. This is then compared to the timeline for controlled release tests conducted for each technology in Figure 1b, showing that most of these controlled tests were carried out at distinct locations and time blocks that differ from the field campaigns. The controlled release test locations are chosen to offer suitable ground conditions, remain well away from urban areas and other methane emitters, and provide convenient access for the instrument crews. For example, the performance characteristics for Carbon Mapper have been developed by testing in Colorado, Arizona, Wyoming and California while Figure 1a shows it has been extensively deployed across various basins throughout the year.[29,33] The PoD equations for Bridger GML have been developed from controlled releases in Texas, Montana, California, and British Columbia.[27] Additionally, these controlled releases were held over a few weeks in particular months as shown in Figure 1b. The fact that testing locations and field campaigns may or may not coincide implies that a detailed comparison of each technology's performance across varying geographic and environmental conditions is necessary to assess potential discrepancies. For instance, controlled release testing done at the METEC facility in Colorado may not be representative of a field campaign undertaken in the Appalachian or the Permian Basin. Colorado has high elevation, low humidity, and strong winds while the Appalachian Basin has forest covered terrain with mean annual wind speed of <3 m/s. The Permian Basin has a flat semiarid terrain with sparse vegetation and clear skies with no terrain interference to hinder emissions detection throughout the year.

3.2. Performance of Methane Detection Technologies under Varying Wind Conditions

Figures 2a and b show the variation in detection performance of Carbon Mapper for measurement campaigns in the fall and summer season respectively under varying wind conditions. The bottom 10th percentile of the emissions detected across the wind speed bins show an increasing trend in both the fall and summer seasons, though there are no distinct operational differences that otherwise explain a change in the true emissions distribution available during observation. In the summer, the bottom 10th percentile of emissions in the 0−4 m/s wind speed bin have a median value around 25 kg/h, increasing to approximately 120 kg/h in the 8−9 m/s bin. In the fall, emission detection trends rise similarly with wind speed, starting from a median of about 30 kg/h in the 0−2 m/s wind speed bin and reaching around 90 kg/h in the 10−12 m/s bin. The best fit line for the median of the lowest 10th percentile emissions has a slope between 12 and 13 kg/h per m/s for both the seasons. This demonstrates that as wind speed increases, the field performance threshold is higher. Even with a difference of approximately 10% between the slopes of the best fit lines, we demonstrate that there is a field performance threshold with wind being the dominant factor in the Permian Basin. The higher R^2 and narrower interquartile ranges at each fall bin may point to the effect of solar irradiance affecting detection performance of the passive Carbon Mapper sensor.

https://doi.org/10.1021/acsestair.5c00437
ACS EST Air XXXX, XXX, XXX−XXX

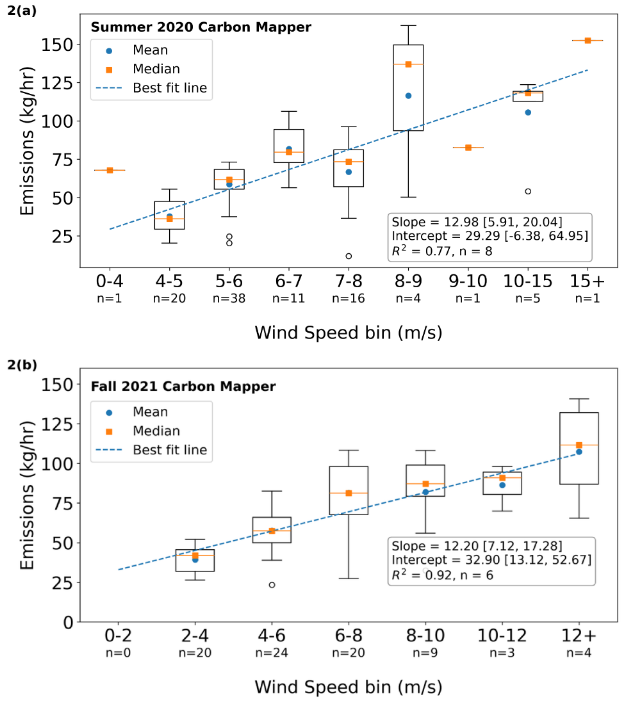

Figure 2. (a) and (b): The bottom 10th percentile of emissions detected by Carbon Mapper as a function of wind speed over the Permian Basin in Summer 2020 and Fall 2021, respectively. Line segments in some bins indicate insufficient data. The horizontal axes represent the different wind distribution profiles of the two seasons. The best fit line is obtained using an ordinary least-squares (OLS) regression.

Figure 3 shows the variation in detection performance with local wind speed for Bridger GML across field campaigns in the Permian Basin. We do not consider the seasonal effect for Bridger GML as the measurement campaigns were conducted through 2021−22 with no clear seasonal demarcation. Though Bridger has a much lower minimum detection limit compared to Carbon Mapper, regression of the median emissions at each bin shows a similar increasing trend in emissions with wind speed. Median emission rates for the bottom 10th percentile increased from 1.0 kg/h when the wind speed is between 0 and 2 m/s to about 2.5 kg/h for winds in the 10−12 m/s bin. The overall dependence on the local wind speed is 0.24 kg/h per m/s meaning a 5 m/s increase in wind speed increases the field threshold by 1.2 kg/h. For example, under field conditions, at wind speeds around 8 m/s the lower tail of the distribution lies above ∼2 kg/h, whereas at wind speeds below 6 m/s this part of the distribution extends below 2 kg/h meaning consistent detection of these emissions. However, individual detections at small emission rates (<2 kg/h) do occur in all wind speed bins.

Overall, both technologies show a positive correlation between wind speed and detected emissions with varying degrees of sensitivity. Carbon Mapper shows a much steeper dependence of reported emission rate on wind speed compared to Bridger GML which indicates a greater sensitivity to wind speed. The increase in emissions with wind speed is more uniform across individual wind-speed bins for Carbon Mapper, whereas Bridger GML shows larger bin-to-bin variability. For Bridger GML, the dependence of performance measurement on wind speed is higher for wind speeds above 6 m/s compared to wind speeds below this.

Prior bottom-up studies that quantified emissions using Hi-Flow samplers have identified emitters that are significantly below the detection threshold of aerial survey technologies. So, the lower tail of the detected emissions in each wind-speed bin is determined by the technology's detection performance near its detection threshold rather than by the full underlying distribution. The 10th percentile of detected emissions thus acts as a practical indicator of a lower bound for reliably detected sources in that bin. This helps us analyze how factors like wind speed affect an instrument's detection capability. Additionally, the maximum emissions detected by both technologies do not differ significantly, and they capture high-emission rate sources (superemitters) reliably.

3.3. Comparative Analysis of Field and Theoretical Detection Performance

Figures 4a and b show a comparison between the 90% PoD line based on controlled release tests and the bottom 10th percentile detected emissions in the field by AVIRIS-NG (Carbon Mapper) for the summer and fall campaigns, respectively. The analyses here use all detected emissions

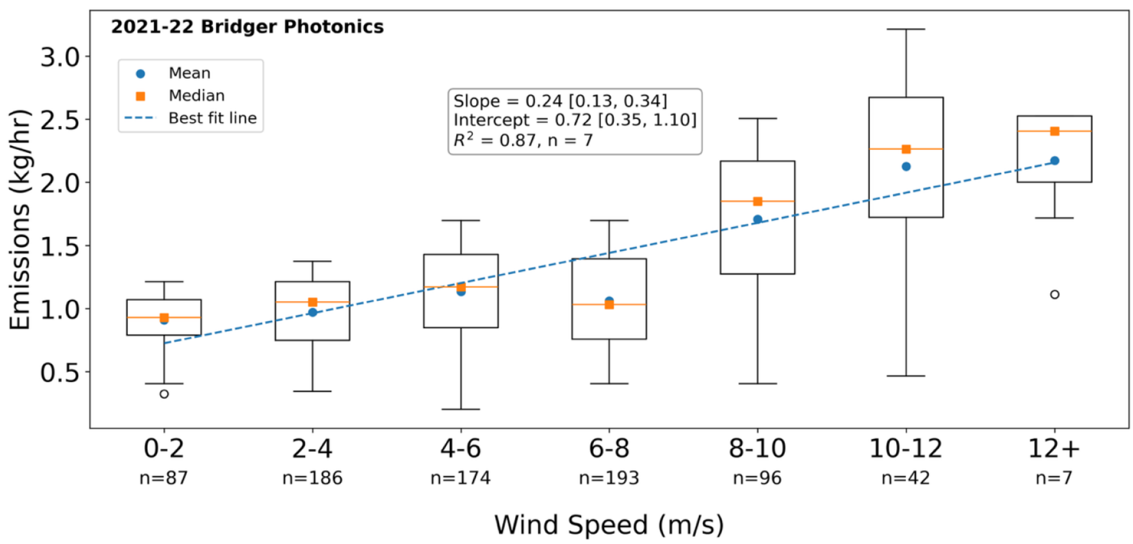

Figure 3. Bottom 10th percentile of emissions detected by Bridger GML as a function of wind speed over the Permian Basin.

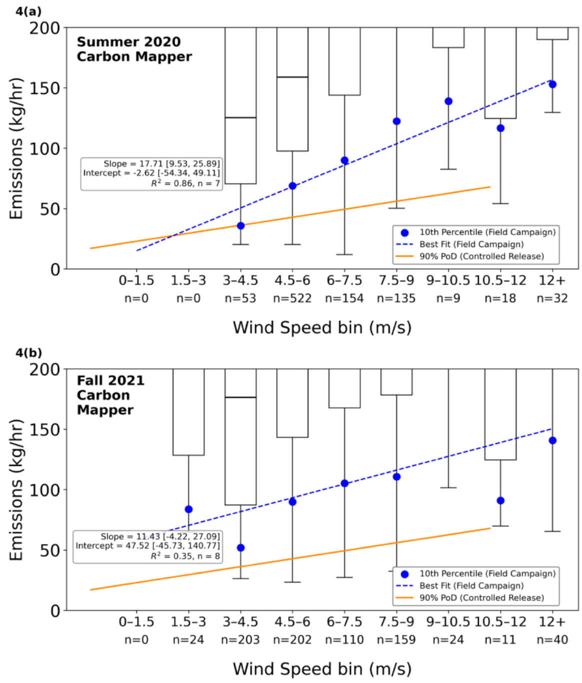

Figure 4. (a) and (b): The difference in methane detection between controlled releases and field campaigns in the Permian Basin for Carbon Mapper in the Summer and Fall, respectively. The orange line represents the 90% PoD over the Permian Basin, and the blue dot indicates the 10th percentile of the detected emissions during the aerial measurement campaigns over the Permian Basin.

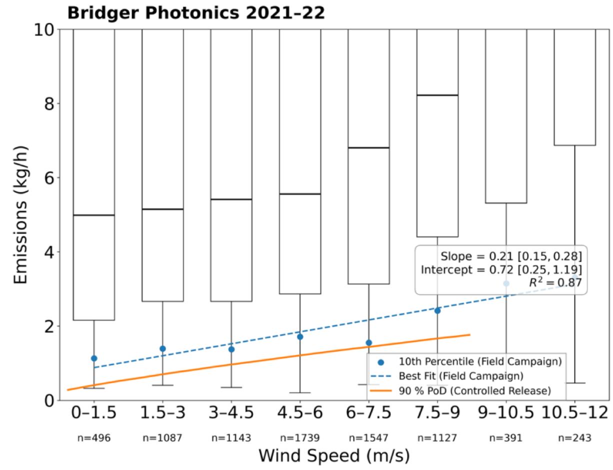

Figure 5. Difference in methane detection between controlled releases and field campaigns in the Permian Basin for Bridger GML. The orange line represents the 90% PoD over the Permian Basin, and the blue dot indicates the 10th percentile of the detected emissions during the aerial measurement campaigns over the Permian Basin. Values labeled n below each box indicate the number of detections (sample size) included in that wind-speed bin.

across the full range of source strengths while Section 3.2focuses only on the lowest 10% of detected emissions in each wind-speed bin, i.e., detections near the field performance threshold. In the summer, the relative difference remains close to zero at low wind speeds (3−4.5 m/s) but increases to more than 30 kg/h at 10 m/s. The slope of the best fit line shows an increase in the field performance threshold of 18.5 kg/h per m/s increase in wind speed for the lowest 10th percentile of emissions. The expected rate of the increase of minimum detection limit from the 90% PoD line is approximately 6.6 kg/h per m/s. In fall conditions, the difference in field performance to the 90% PoD line is more uniform (25−35 kg/h) across the wind speed bins. Although emissions threshold rose with wind speed bin, the slope of 13 kg/h per m/s was shallower than in the summer with a greater scatter and wider interquartile range. To evaluate whether the difference in slopes is statistically significant across the two seasons, we conducted a hypothesis test comparing the fitted summer and fall slopes. The estimated difference in slopes is not statistically significant at the 95% confidence level (i.e., the 95% confidence interval for the slope difference includes zero). This discrepancy indicates that the field performance of AVIRIS-NG (Carbon Mapper) diverges from the model predictions and suggests that PoD models should incorporate not only wind speed but also additional meteorological conditions (e.g., temperature, humidity, boundary-layer structure) and surface properties such as surface reflectance and terrain type (albedo).

Figure 5 shows the comparison between the field derived 10th percentile of detected emissions and the 90% PoD line for Bridger GML. At low wind speeds (~2 m/s), the field performance threshold for Bridger GML (~1 kg/h) is more than twice the minimum detection limit (0.4 kg/h) predicted by the 90% PoD threshold. This high relative disparity suggests that at lower wind speeds, Bridger GML is less effective at achieving the minimum detection limit determined by the PoD model. The relative difference between the field performance threshold and the PoD curve decreases at higher wind speeds (>4 m/s). This is because the field-derived slope (0.21 kg/h per m/s) is shallower than the PoD curve (0.29 kg/h per m/s). A *t*-test comparing the two slopes shows that this difference is statistically significant at the 95% confidence level (*t*-statistic = −2.22). This indicates that as wind speed increases, the minimum plume strength required for a detection grows more gradually in field conditions than predicted by controlled-test performance.

The comparison between the 90% PoD line and the empirical 10th percentile of detected emissions is conducted to evaluate how well theoretical detection performance translates into real-world conditions. Qualitatively, if the 90% PoD line is consistently below the 10th percentile of detected emissions, it suggests that the minimum detection limit based on the PoD models is overestimated compared to observed performance in field measurement campaigns. Overall, in the fall season the AVIRIS-NG field-based 10th-percentile trend is offset by a roughly constant amount across wind speed bins. Whereas, in the summer the discrepancy between the field data and the PoD curve increases with wind speed, potentially reflecting seasonal environmental influences on detection efficacy and the PoD model being developed by controlled release of methane during fall. While the PoD models provide a robust framework for expected performance, real-world factors continue to impact detection capability.

3.4. Field Validation of Detection Sensitivity: Comparison with PoD Model Predictions

In the following analysis, we combine field campaign data collected across two seasons for AVIRIS-NG and derive local wind speed at each plume location. For each observed wind speed, the detected emissions are identified and plotted to identify the trend for a field performance threshold. A 90%

confidence interval line is added to the plot for statistical robustness. A theoretical slope of 0.1201 is calculated from the PoD function described in eq 1 to establish a benchmark for the expected detection sensitivity. We calculate this slope for a fixed flight altitude of 3000 m and 90% probability of detection and then compare the theoretical slope with data from the field campaign in the Permian Basin. Figure 6a shows the variation in emissions with wind speed with the best fit line and 90% confidence bands. We observe that in the field, the slope of the log of emissions versus wind speed is in the range [0.1541, 0.2023] with 95% confidence. This shows that the trend of the log-linear relationship between the emissions and wind speed is linear as expected from the PoD function. However, at each wind speed there were emission measurements that were likely missed due to a variability in the detection performance under changing local meteorological conditions.

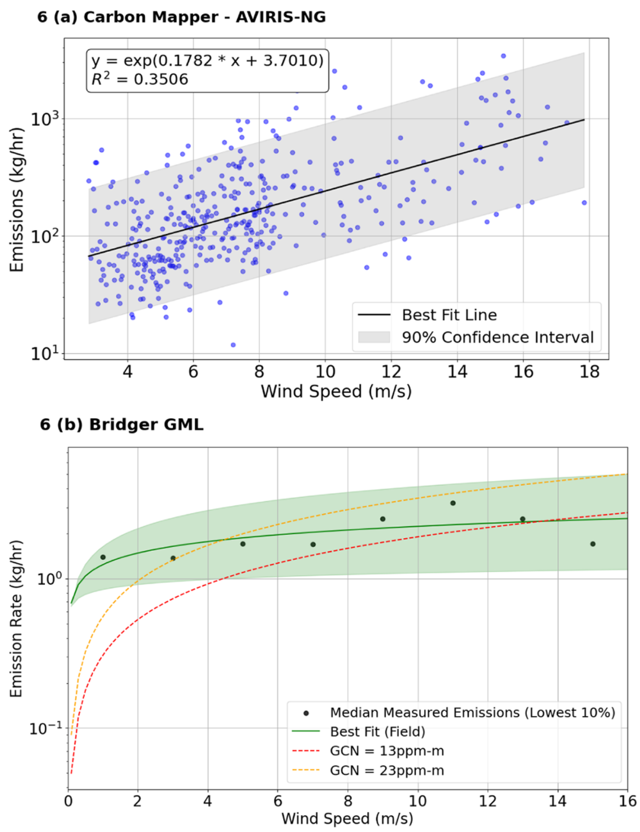

Figure 6. (a): Best fit line on a log-linear scale and 90% confidence band for emissions vs wind speed for Carbon Mapper in the Permian Basin. For each local wind speed, all the measured emissions during the campaign (blue) along with the best fit line (black) are shown. (b): Best fit and 90% confidence band for emissions vs wind speed for Bridger GML in the Permian Basin. The dashed lines represent the minimum detection limit at 90% PoD for each wind speed with GCNs of 13 ppm-m (red) and 23 ppm-m (orange) respectively. The median of the lowest 10% measured emissions (green) along with the best fit curve and the confidence interval (green) show the field performance threshold.

We compare the minimum detection limit from the deployment invariant model for Bridger GML with the detections observed from the field campaigns. The median emissions of the lowest 10% emissions in each wind speed bin are compared to the predicted emissions for two gas concentration noise values—13 ppm-m and 23 ppm-m. Figure 6b shows the variation of emissions with wind speed for field detected emissions compared to the minimum detection limit for the two GCN values. At low wind speeds (<5 m/s), the observed emissions curve shown in green, are consistently higher than both the predicted curves. At 3.5 m/s, the observed emissions are 45% higher than predictions for GCN = 13 ppm-m, and 4 times higher than the predictions for GCN = 23 ppm-m. At higher wind speeds, while discrepancies remain, the predictions for GCN = 13 ppm-m provide a better approximation of observed emissions compared to GCN = 23 ppm-m. At wind speeds of 8–9 m/s, the observed emissions are approximately 3.5–4.0 kg/h, which are 15–20% higher than the predicted emissions for GCN = 13 ppm-m (3.0 kg/h) and 3 times higher for GCN = 23 ppm-m (0.8–1.0 kg/h). At wind speeds above 10–11 m/s, fewer emissions are observed. This is likely due to limited measurements on very windy days, making comparisons with predicted emissions at very high wind speeds inconclusive. Overall, the analysis highlights the challenges in accurately predicting detection performance under varying wind conditions for Bridger GML, particularly at low wind speeds where real-world variability may not be fully represented in the model.

Finally, the higher slope observed in the field results for AVIRIS-NG and the discrepancy observed in the slopes for Bridger GML, even accounting for the 95% confidence interval for both the aerial technologies, highlight a key difference. While the field trends follow the overall relationship predicted by the PoD models, the actual detection performance in the field is overestimated since it is based on detection performance developed during controlled release studies. It also suggests that field calibration is essential for accurately predicting technology performance across varied conditions.

4. DISCUSSION AND CONCLUSION

This study presents several key findings on the performance of methane measurement technologies in real-world conditions. First, an analysis of basin wide methane detection campaigns shows that for both AVIRIS-NG and Bridger GML, the minimum detection threshold increases with local wind speed. The minimum detection threshold of AVIRIS-NG over the two detection seasons increased by up to three times as the local wind speed increased from 2 to 10 m/s. For Bridger GML, the minimum detection threshold more than doubles over the same wind speed range. Second, the comparison between measured emissions from field data and emissions expected to be detected from PoD curves for the two technologies shows significant discrepancies. This discrepancy is observed near both lower and upper bounds of wind speed. Third, on validating the field data against deployment-invariant PoD equations, our findings indicate that these equations tend to overestimate detection performance. The PoD equations are found to be useful in showing the general trend that emissions from field campaigns follow, yet the observed emissions are largely higher than predicted emissions at each wind speed. Our findings demonstrate the unique challenges posed by atmospheric variability, such as wind speed which affect field campaigns in ways that controlled releases do not fully capture. This reconciliation helps refine testing protocols and improvement of methane emissions inventories at the facility, regional, and basin scales.

A key implication of this study is the quantification of methane emissions that are likely missed under operational conditions compared to idealized detection scenarios. To

https://doi.org/10.1021/acsestair.5c00437
ACS EST Air XXXX, XXX, XXX−XXX

assess these missed emissions, we conducted an analysis to estimate the total methane emissions that would have been detected under more favorable conditions for Carbon Mapper. Our approach involves classifying emissions into wind speed bins based on the local wind speed distribution for the Permian Basin. Each wind bin is assigned a percentage of total emissions based on the duration that the particular wind speed occurred during the measurement campaign. This ensures that the allocation reflects realistic environmental conditions encountered during field campaigns.

For each wind-speed bin, we define a field performance threshold as the median of the lowest 10% detected emissions in that bin. This is used as an empirical metric for the performance near the detection threshold used for this study and does not correspond to a field based 90% PoD curve for a particular technology. The assumptions and calculation steps are described in detail in the SI Section 7. To determine the portion of emissions missed, we use the cumulative distribution function (CDF) of emissions, developed by Kunkel et al. for the Permian Basin.[8] The missed emission fraction for each bin is calculated based on the proportion of emissions falling below the detection threshold. We determine the total fraction of emissions that went undetected by aggregating the missed emissions across all wind bins. Figures 7a and b show the percentage of total emissions that go undetected in each windspeed bin with the cumulative share of missed emissions as wind speed increases for summer and fall season measurement campaigns in the Permian Basin. Approximately 20% of methane emissions in the Permian Basin are cumulatively missed under fall and summer season field conditions for AVIRIS-NG compared to what could potentially be captured under more favorable conditions. The proportion of emissions that remain undetected varies by wind speed bin. In the summer season, most emissions are missed in the 4−6 m/s bins. In fall, approximately 5 percentage points of emissions are missed in the 4−6 m/s and 6−8 m/s bins, whereas about 3 percentage points are missed in the 2−4 m/s and 8−10 m/s bins. At higher wind speeds (>8 m/s) the incremental missed emissions per bin drop below 1 percentage point for both the seasons which could be due to a lower number of plumes available to detect at these wind speeds.

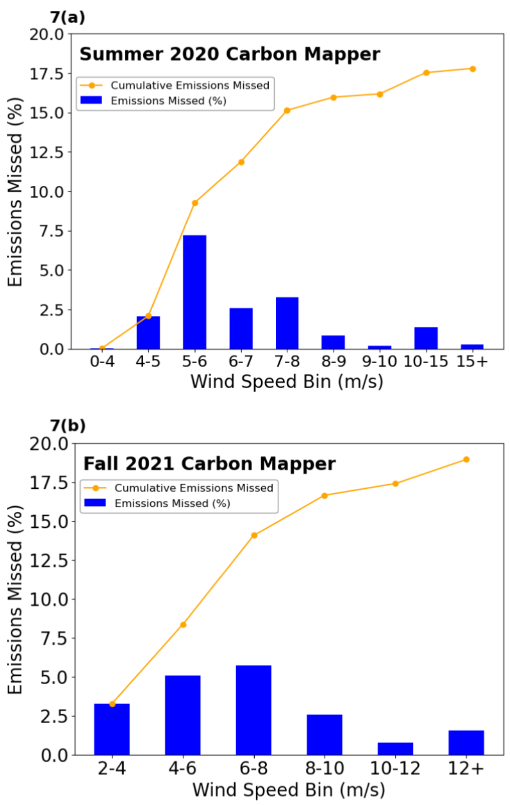

Figure 7. (a) and (b): Blue bars show the percentage of total field-measured emissions that Carbon Mapper failed to detect in each wind-speed bin and the orange line represents the cumulative fraction of missed emissions as wind speed increases during the aerial measurement campaigns (summer 2020 and fall 2021) over the Permian Basin. The missed emissions are relative to the total emissions from the basin-level PDF at each wind speed bin.

Another implication relates to the sensitivity of methane emission estimates to wind speed measurement errors. To assess the extent to which errors in wind speed affect the performance of two detection technologies, we conducted an analysis by introducing a ±5% and ±10% variation in the measured wind speeds for both technologies. Wind speeds are binned into increments of 0.05 m/s, and a probable emission rate is assigned to each wind speed based on a Monte Carlo simulation of existing emission rates. This probabilistic approach ensures that the analysis reflects the natural variability in emissions typically observed in field settings.

The results show that there is a difference in sensitivity to wind speed uncertainty. Carbon Mapper exhibits a wider change in estimated emissions compared to Bridger. This finding presents implications for the design of field monitoring strategies, particularly regarding the use of representative wind speeds. For Bridger, a representative airport wind speed is used to analyze the dependence of emissions on various meteorological factors. While this approach works for Bridger's technology, using a similar method for other technologies such as Carbon Mapper may yield different results due to its heigher sensitivity to wind speed changes. Supporting figures are provided in the SI Section S5 (Figures S10 and S11). So, methane monitoring campaigns should be designed to account for the wind speed dependency of different technologies. This is essential for ensuring consistency in methane inventories and improving the reliability of methane detection and quantification across different technologies.

Our results demonstrate a systematic underestimation of low-magnitude emissions in field campaigns compared to controlled-release experiments. The discrepancy is particularly pronounced in regions with highly variable wind speeds with emissions being missed at lower and higher wind speeds during limited duration aerial surveys. This observed difference between the field performance threshold and the minimum detection limit from controlled release results can be attributed to the change in a technology's performance due to environmental variability present in operational settings. Specifically, high wind speeds increase plume dispersion, making it harder for remote sensing technologies to detect low-magnitude emissions. Meanwhile, controlled release experiments are conducted under relatively stable and controlled conditions, leading to better algorithm performance and reduced uncertainty in measurements.

We focus on the Permian Basin due to the availability of extensive data sets from repeat surveys that allow for a more detailed analysis of the impact of environmental variability on detection capabilities. Given the Permian Basin's status as one of the largest sources of methane emissions in the U.S., the

https://doi.org/10.1021/acsestair.5c00437
ACS EST Air XXXX, XXX, XXX−XXX

insights derived from this study have significant relevance for broader methane monitoring initiatives. While the methods and frameworks developed in this study should extend to other basins, differences in emission characteristics and operational practices across regions may influence detection outcomes. Future research can apply these methods to other basins to validate the findings and assess potential region-specific variations in methane emission distributions and detection sensitivities.

ASSOCIATED CONTENT

Supporting Information

The Supporting Information is available free of charge at https://pubs.acs.org/doi/10.1021/acsestair.5c00437.

Performance of Bridger Photonics Gas Mapping LiDAR (GML) across additional basins; dependence of Carbon Mapper detection performance on local solar azimuth angle, solar irradiance, and temperature; effect of wind speed measurement location and wind speed measurement error on emissions detection; spatial and time-of-day variation in Carbon Mapper measurements; quantification of potentially missed emissions; sensitivity analyses for wind speed bin widths and percentile threshold selection; and supplementary analyses of the prevalence of small detections with increasing wind speed for Bridger GML (PDF)

AUTHOR INFORMATION

Corresponding Author

Arvind P. Ravikumar – *Center for Energy and Environmental Systems Analysis (CEESA), The University of Texas at Austin, Austin, Texas 78712, United States; Energy Emissions Modeling and Data Lab (EEMDL) and Department of Petroleum and Geosystems Engineering, The University of Texas at Austin, Austin, Texas 78712, United States;* orcid.org/0000-0001-8385-6573; Email: arvind.ravikumar@austin.utexas.edu

Authors

Saahil Gupta – *Center for Energy and Environmental Systems Analysis (CEESA), The University of Texas at Austin, Austin, Texas 78712, United States; Energy Emissions Modeling and Data Lab (EEMDL) and Department of Petroleum and Geosystems Engineering, The University of Texas at Austin, Austin, Texas 78712, United States;* orcid.org/0000-0002-8606-9062

Erin Tullos – *Center for Energy and Environmental Systems Analysis (CEESA), The University of Texas at Austin, Austin, Texas 78712, United States; Energy Emissions Modeling and Data Lab (EEMDL), The University of Texas at Austin, Austin, Texas 78712, United States*

David Lyon – *Environmental Defense Fund, Austin, Texas 78701, United States*

Haoming Ma – *Center for Energy and Environmental Systems Analysis (CEESA), The University of Texas at Austin, Austin, Texas 78712, United States; Energy Emissions Modeling and Data Lab (EEMDL) and Department of Petroleum and Geosystems Engineering, The University of Texas at Austin, Austin, Texas 78712, United States*

Complete contact information is available at: https://pubs.acs.org/10.1021/acsestair.5c00437

Author Contributions

S.G.: Conceptualization, Methodology, Validation, Formal analysis, Data curation, Writing—original draft, Writing—review and editing, Visualization. E.T.: Conceptualization, Validation, Formal analysis, Resources, Writing—review and editing, Supervision. D.L.: Validation, Investigation, Data curation, Resources, Writing—review and editing. H.M.: Validation, Formal analysis, Resources, Writing—review and editing. A.P.R.: Conceptualization, Methodology, Validation, Formal analysis, Resources, Writing—review and editing, Supervision, Project administration, Funding acquisition. All authors have reviewed and approved the published version of the manuscript.

Notes

The authors declare no competing financial interest.

ACKNOWLEDGMENTS

This work was funded in part by the US Department of Energy grant DE-FE0032326 and the Energy Emissions Modeling and Data Lab.

REFERENCES

(1) United Nations Environment Programme. *An Eye on Methane 2024: Invisible but Not Unseen: How Data-Driven Tools Can Turn the Tide on Methane Emissions – If We Use Them.* United Nations Environment Programme, 2024. .

(2) Calvin, K.; Dasgupta, D.; Krinner, G.; Mukherji, A.; Thorne, P. W.; Trisos, C.; Romero, J.; Aldunce, P.; Barrett, K.; Blanco, G. et al. *Climate Change 2023: Synthesis Report. Contribution of Working Groups I, II and III to the Sixth Assessment Report of the Intergovernmental Panel on Climate Change* Lee, H.; Romero, J. Eds. Intergovernmental Panel on Climate Change (IPCC) Geneva 2023 .

(3) Hmiel, B.; Petrenko, V. V.; Dyonisius, M. N.; Buizert, C.; Smith, A. M.; Place, P. F.; Harth, C.; Beaudette, R.; Hua, Q.; Yang, B.; Vimont, I.; Michel, S. E.; Severinghaus, J. P.; Etheridge, D.; Bromley, T.; Schmitt, J.; Faïn, X.; Weiss, R. F.; Dlugokencky, E. Preindustrial 14CH4 Indicates Greater Anthropogenic Fossil CH4 Emissions. *Nature* **2020**, *578* (7795), 409–412.

(4) International Energy Agency (IEA). *Global Methane Tracker_Documentation - 2024 Version* International Energy Agency (IEA). 2023

(5) GMP. *Factsheet: 2024 Global Methane Pledge Ministerial.* https://www.globalmethanepledge.org/news/factsheet-2024-global-methane-pledge-ministerial.

(6) United Nations Environment Programme. *The Oil and Gas Methane Partnership 2.0.* 2025. https://www.ogmpartnership.org/sites/default/files/resources/2025-04/OGMP-2.0-Introduction.pdf.

(7) Frankenberg, C.; Thorpe, A. K.; Thompson, D. R.; Hulley, G.; Kort, E. A.; Vance, N.; Borchardt, J.; Krings, T.; Gerilowski, K.; Sweeney, C.; Conley, S.; Bue, B. D.; Aubrey, A. D.; Hook, S.; Green, R. O. Airborne Methane Remote Measurements Reveal Heavy-Tail Flux Distribution in Four Corners Region. *Proc. Natl. Acad. Sci. U. S. A* **2016**, *113* (35), 9734–9739.

(8) Kunkel, W. M.; Carre-Burritt, A. E.; Aivazian, G. S.; Snow, N. C.; Harris, J. T.; Mueller, T. S.; Roos, P. A.; Thorpe, M. J. Extension of Methane Emission Rate Distribution for Permian Basin Oil and Gas Production Infrastructure by Aerial LiDAR. *Environ. Sci. Technol* **2023**, *57* (33), 12234–12241.

(9) Duren, R. M.; Thorpe, A. K.; Foster, K. T.; Rafiq, T.; Hopkins, F. M.; Yadav, V.; Bue, B. D.; Thompson, D. R.; Conley, S.; Colombi, N. K.; Frankenberg, C.; McCubbin, I. B.; Eastwood, M. L.; Falk, M.; Herner, J. D.; Croes, B. E.; Green, R. O.; Miller, C. E. California's Methane Super-Emitters. *Nature* **2019**, *575* (7781), 180–184.

(10) Cusworth, D. H.; Duren, R. M.; Thorpe, A. K.; Olson-Duvall, W.; Heckler, J.; Chapman, J. W.; Eastwood, M. L.; Helmlinger, M. C.; Green, R. O.; Asner, G. P.; Dennison, P. E.; Miller, C. E.

Intermittency of Large Methane Emitters in the Permian Basin. *Environ. Sci. Technol. Lett* **2021**, *8* (7), 567−573.
(11) Hmiel, B.; Lyon, D. R.; Warren, J. D.; Yu, J.; Cusworth, D. H.; Duren, R. M.; Hamburg, S. P. Empirical Quantification of Methane Emission Intensity from Oil and Gas Producers in the Permian Basin. *Environ. Res. Lett* **2023**, *18* (2), 024029.
(12) Esparza, Á. E.; Ebbs, M.; De Toro Eadie, N.; Roffo, R.; Monnington, L. Utilizing Remote Sensing and Data Analytics Techniques to Detect Methane Emissions from the Oil and Gas Industry and Assist with Sustainability Metrics. *SPE Prod. Oper* **2023**, *38* (4), 640−650.
(13) Yu, J.; Hmiel, B.; Lyon, D. R.; Warren, J.; Cusworth, D. H.; Duren, R. M.; Chen, Y.; Murphy, E. C.; Brandt, A. R. Methane Emissions from Natural Gas Gathering Pipelines in the Permian Basin. *Environ. Sci. Technol. Lett* **2022**, *9* (11), 969−974.
(14) Daniels, W. S.; Wang, J. L.; Ravikumar, A. P.; Harrison, M.; Roman-White, S. A.; George, F. C.; Hammerling, D. M. Toward Multiscale Measurement-Informed Methane Inventories: Reconciling Bottom-Up Site-Level Inventories with Top-Down Measurements Using Continuous Monitoring Systems. *Environ. Sci. Technol* **2023**, *57* (32), 11823−11833.
(15) Wang, J. L.; Daniels, W. S.; Hammerling, D. M.; Harrison, M.; Burmaster, K.; George, F. C.; Ravikumar, A. P. Multiscale Methane Measurements at Oil and Gas Facilities Reveal Necessary Frameworks for Improved Emissions Accounting. *Environ. Sci. Technol* **2022**, *56* (20), 14743−14752.
(16) Pétron, G.; Karion, A.; Sweeney, C.; Miller, B. R.; Montzka, S. A.; Frost, G. J.; Trainer, M.; Tans, P.; Andrews, A.; Kofler, J.; Helmig, D.; Guenther, D.; Dlugokencky, E.; Lang, P.; Newberger, T.; Wolter, S.; Hall, B.; Novelli, P.; Brewer, A.; Conley, S.; Hardesty, M.; Banta, R.; White, A.; Noone, D.; Wolfe, D.; Schnell, R. A New Look at Methane and Nonmethane Hydrocarbon Emissions from Oil and Natural Gas Operations in the Colorado Denver-Julesburg Basin. *J. Geophys. Res. Atmos* **2014**, *119* (11), 6836−6852.
(17) Barkley, Z. R.; Lauvaux, T.; Davis, K. J.; Deng, A.; Miles, N. L.; Richardson, S. J.; Cao, Y.; Sweeney, C.; Karion, A.; Smith, M.; Kort, E. A.; Schwietzke, S.; Murphy, T.; Cervone, G.; Martins, D.; Maasakkers, J. D. Quantifying Methane Emissions from Natural Gas Production in North-Eastern Pennsylvania. *Atmos. Chem. Phys* **2017**, *17* (22), 13941−13966.
(18) Peischl, J.; Eilerman, S. J.; Neuman, J. A.; Aikin, K. C.; de Gouw, J.; Gilman, J. B.; Herndon, S. C.; Nadkarni, R.; Trainer, M.; Warneke, C.; Ryerson, T. B. Quantifying Methane and Ethane Emissions to the Atmosphere From Central and Western U.S. Oil and Natural Gas Production Regions. *J. Geophys. Res. Atmos* **2018**, *123* (14), 7725−7740.
(19) Chen, Y.; Sherwin, E. D.; Berman, E. S. F.; Jones, B. B.; Gordon, M. P.; Wetherley, E. B.; Kort, E. A.; Brandt, A. R. Quantifying Regional Methane Emissions in the New Mexico Permian Basin with a Comprehensive Aerial Survey. *Environ. Sci. Technol* **2022**, *56* (7), 4317−4323.
(20) Permian MAP. *Environmental Defense Fund* Permian MAP 2019 https://data.permianmap.org/.
(21) Stokes, S.; Tullos, E.; Morris, L.; Cardoso-Saldaña, F. J.; Smith, M.; Conley, S.; Smith, B.; Allen, D. T. Reconciling Multiple Methane Detection and Quantification Systems at Oil and Gas Tank Battery Sites. *Environ. Sci. Technol* **2022**, *56* (22), 16055−16061.
(22) Williams, J. P.; Omara, M.; Himmelberger, A.; Zavala-Araiza, D.; MacKay, K.; Benmergui, J.; Sargent, M.; Wofsy, S. C.; Hamburg, S. P.; Gautam, R. Small Emission Sources in Aggregate Disproportionately Account for a Large Majority of Total Methane Emissions from the US Oil and Gas Sector. *Atmospheric Chem. Phys.* **2025**, *25* (3), 1513−1532.
(23) Ravikumar, A. P.; Sreedhara, S.; Wang, J.; Englander, J.; Roda-Stuart, D.; Bell, C.; Zimmerle, D.; Lyon, D.; Mogstad, I.; Ratner, B.; Brandt, A. R. Single-Blind Inter-Comparison of Methane Detection Technologies − Results from the Stanford/EDF Mobile Monitoring Challenge. *Elem. Sci. Anthr* **2019**, *7*, 37.
(24) Liu, Y.; Paris, J.-D.; Broquet, G.; Bescós Roy, V.; Meixus Fernandez, T.; Andersen, R.; Russu Berlanga, A.; Christensen, E.; Courtois, Y.; Dominok, S.; Dussenne, C.; Eckert, T.; Finlayson, A.; Fernández de la Fuente, A.; Gunn, C.; Hashmonay, R.; Grigoleto Hayashi, J.; Helmore, J.; Honsel, S.; Innocenti, F.; Irjala, M.; Log, T.; Lopez, C.; Cortés Martínez, F.; Martinez, J.; Massardier, A.; Nygaard, H. G.; Agregan Reboredo, P.; Rousset, E.; Scherello, A.; Ulbricht, M.; Weidmann, D.; Williams, O.; Yarrow, N.; Zarea, M.; Ziegler, R.; Sciare, J.; Vrekoussis, M.; Bousquet, P. Assessment of Current Methane Emission Quantification Techniques for Natural Gas Midstream Applications. *Atmos. Meas. Tech.* **2024**, *17* (6), 1633−1649.
(25) Morales, R.; Ravelid, J.; Vinkovic, K.; Korbeń, P.; Tuzson, B.; Emmenegger, L.; Chen, H.; Schmidt, M.; Humbel, S.; Brunner, D. Controlled-Release Experiment to Investigate Uncertainties in UAV-Based Emission Quantification for Methane Point Sources. *Atmos. Meas. Tech.* **2022**, *15* (7), 2177−2198.
(26) Johnson, M. R.; Tyner, D. R.; Szekeres, A. J. Blinded Evaluation of Airborne Methane Source Detection Using Bridger Photonics LiDAR. *Remote Sens. Environ* **2021**, *259*, 112418.
(27) Thorpe, M. J.; Kreitinger, A.; Altamura, D. T.; Dudiak, C. D.; Conrad, B. M.; Tyner, D. R.; Johnson, M. R.; Brasseur, J. K.; Roos, P. A.; Kunkel, W. M.; et al. Deployment-invariant probability of detection characterization for aerial LiDAR methane detection. *Remote Sens. Environ.* **2024**, *315*, 114435.
(28) Sherwin, E. D.; Chen, Y.; Ravikumar, A. P.; Brandt, A. R. Single-Blind Test of Airplane-Based Hyperspectral Methane Detection via Controlled Releases. *Elem. Sci. Anthr* **2021**, *9* (1), 00063.
(29) El Abbadi, S. H.; Chen, Z.; Burdeau, P. M.; Rutherford, J. S.; Chen, Y.; Zhang, Z.; Sherwin, E. D.; Brandt, A. R. Technological Maturity of Aircraft-Based Methane Sensing for Greenhouse Gas Mitigation. *Environ. Sci. Technol* **2024**, *58* (22), 9591−9600.
(30) Worden, J.; Elder, C.; Poulter, B.; Balashov, N. *Commercial Satellite Data Acquisition Program GHGSat Emission Quality Assessment Report*. Goddard Space Flight Center 2024.
(31) Cusworth, D. H.; Bon, D. M.; Varon, D. J.; Ayasse, A. K.; Asner, G. P.; Heckler, J.; Sherwin, E. D.; Biraud, S. C.; Duren, R. Duration of Super-Emitting Oil & Gas Methane Sources, **2025** *17*, 2011 .
(32) Conrad, B. M.; Tyner, D. R.; Johnson, M. R. Robust Probabilities of Detection and Quantification Uncertainty for Aerial Methane Detection: Examples for Three Airborne Technologies. *Remote Sens. Environ* **2023**, *288*, 113499.
(33) Thorpe, A. K.; Frankenberg, C.; Aubrey, A. D.; Roberts, D. A.; Nottrott, A. A.; Rahn, T. A.; Sauer, J. A.; Dubey, M. K.; Costigan, K. R.; Arata, C.; Steffke, A. M.; Hills, S.; Haselwimmer, C.; Charlesworth, D.; Funk, C. C.; Green, R. O.; Lundeen, S. R.; Boardman, J. W.; Eastwood, M. L.; Sarture, C. M.; Nolte, S. H.; Mccubbin, I. B.; Thompson, D. R.; McFadden, J. P. Mapping Methane Concentrations from a Controlled Release Experiment Using the next Generation Airborne Visible/Infrared Imaging Spectrometer (AVIRIS-NG). *Remote Sens. Environ* **2016**, *179*, 104−115.
(34) Bell, C.; Rutherford, J.; Brandt, A.; Sherwin, E.; Vaughn, T.; Zimmerle, D. Single-Blind Determination of Methane Detection Limits and Quantification Accuracy Using Aircraft-Based LiDAR. *Elem. Sci. Anthr* **2022**, *10* (1), 00080.
(35) Meteostat Developers. *Meteostat Python Library*, 2024. https://github.com/meteostat.
(36) Environmental Defense Fund. *Summer 2020 Sources Detected by GAO - CarbonMapper*, 2022. https://data.permianmap.org/documents/fd9b9e67b95b456694f9ff323d8c0e0d/about Accessed 17 December 2024.
(37) Environmental Defense Fund. *Fall 2021 Sources Detected by GAO - CarbonMapper*, 2022. https://data.permianmap.org/maps/931fc767c48b4f279a138b1e7164ca1c Accessed 17 December 2024.
(38) Thorpe, A. K.; Duren, R. M.; Conley, S.; Prasad, K. R.; Bue, B. D.; Yadav, V.; Foster, K. T.; Rafiq, T.; Hopkins, F. M.; Smith, M. L.; Fischer, M. L.; Thompson, D. R.; Frankenberg, C.; McCubbin, I. B.;

https://doi.org/10.1021/acsestair.5c00437
ACS EST Air XXXX, XXX, XXX−XXX

Eastwood, M. L.; Green, R. O.; Miller, C. E. Methane Emissions from Underground Gas Storage in California. *Environ. Res. Lett* **2020**, *15* (4), 045005.
(39) Omara, M.; Zavala-Araiza, D.; Lyon, D. R.; Hmiel, B.; Roberts, K. A.; Hamburg, S. P. Methane Emissions from US Low Production Oil and Natural Gas Well Sites. *Nat. Commun* **2022**, *13* (1), 2085.
(40) Schwietzke, S.; Harrison, M.; Lauderdale, T.; Branson, K.; Conley, S.; George, F. C.; Jordan, D.; Jersey, G. R.; Zhang, C.; Mairs, H. L.; Pétron, G.; Schnell, R. C. Aerially Guided Leak Detection and Repair: A Pilot Field Study for Evaluating the Potential of Methane Emission Detection and Cost-Effectiveness. *J. Air Waste Manage. Assoc* **2019**, *69* (1), 71−88.
(41) Sherwin, E. D.; Rutherford, J. S.; Zhang, Z.; Chen, Y.; Wetherley, E. B.; Yakovlev, P. V.; Berman, E. S. F.; Jones, B. B.; Cusworth, D. H.; Thorpe, A. K.; Ayasse, A. K.; Duren, R. M.; Brandt, A. R. US Oil and Gas System Emissions from Nearly One Million Aerial Site Measurements. *Nature* **2024**, *627* (8003), 328−334.
(42) Berman, E. S. F.; Wetherley, E. B.; Jones, B. B. *Kairos Aerospace Technical White Paper: Methane Detection*. Kairos Aerospace 2021
(43) Rutherford, J. S.; Sherwin, E. D.; Chen, Y.; Aminfard, S.; Brandt, A. R.Evaluating Methane Emission Quantification Performance and Uncertainty of Aerial Technologies via High-Volume Single-Blind Controlled Releases*arXiv***2023**

https://doi.org/10.1021/acsestair.5c00437
ACS EST Air XXXX, XXX, XXX−XXX